

Lower switching-current density in Ta/(Pt/X)_n/Pt/Co/Ta (X = Ta, Mn, Cu, V, Zr, Bi; n = 3, 4) multilayers based on a domain-wall-depinning model

Shuanghai Wang,^{1,2} Kun He,^{1,2} Yongkang Xu,^{1,2} Zhuoyi Li,^{1,2} Jin Wang,^{1,2} Caitao Li,^{1,2} Xingze Dai,^{1,2}
Jun Du,³ Yong-Lei Wang,⁴ Ronghua Liu^{1,2},⁵ Xianyang Lu^{1,2},⁵ Yongbing Xu,^{1,2,*} and Liang He^{1,2,†}

¹School of Electronic Science and Engineering, Nanjing University, Nanjing 210023, China

²National Key laboratory of spintronics, Nanjing University, Suzhou, 215163, China

³National Laboratory of Solid State Microstructures and Department of Physics, Nanjing University,
Nanjing 210093, China

⁴Research Institute of Superconductor Electronics, School of Electronic Science and Engineering,
Nanjing University, Nanjing 210023, China

⁵Jiangsu Key Laboratory for Nanotechnology, Department of Physics, Nanjing University, Nanjing 210093, China

(Received 12 May 2024; revised 8 July 2024; accepted 8 August 2024; published 29 August 2024)

In recent years, spin-orbit torque (SOT) generated by heavy metal (HM) has garnered increasing attention. However, SOT-magnetic random-access memory based on HM suffers from a low spin Hall angle and high current density. Here, we demonstrate that the critical switching-current density (I_c) in a multilayer structure of Ta/(Pt/Ta)₄/Pt/Co/Ta has been reduced by 79% compared with that of Ta/Pt/Co/Ta, achieving a value of 5.88×10^6 A/cm². This value is considerably low among all reported values in the Pt/Co system literature. The reduction of I_c is accompanied by enhanced dampinglike torque efficiency (β_D) and reduced coercive force (H_c). A perfect linear correlation has been observed between I_c and H_c/β_D , which supports the domain-wall depinning model of the SOT-induced magnetization reversal in this system. Crucially, this linearity extends to several metal dopants possessing the identical superlattice structure. This research offers insights into the future of low-power, high-density magnetic memory technology based on HM materials.

DOI: 10.1103/PhysRevApplied.22.L021002

Spintronic devices that utilize spin-orbit torque (SOT) not only enhance our comprehension of fundamental physics but also provide an effective solution for data writing in magnetic memories and logic computing technologies [1–6]. In the multilayer structure composed of HM and ferromagnetic (FM) layers, the spin-orbit coupling (SOC) of HM generates a transverse spin current as the electron current passes through it. When the spin current is large enough, it interacts with the magnetic moment of the FM layer, resulting in aligning the magnetic moment with the spin direction of the electrons [7–11].

Currently, the application of SOT-based storage devices faces two primary challenges. Firstly, deterministic switching requires the breaking of symmetry, which has been achieved through the application of an external magnetic field [12–14], exchange bias [15,16], crystal structure asymmetry [17,18], tilted anisotropy [19,20], wedge-shaped growth of heavy metals [21,22], and tilted

annealing [23], etc. Secondly, I_c is excessively high. To reduce I_c , attention has been focused on enhancing β_D , which involves the utilization of topological materials with very strong SOC, such as Bi₂Se₃ [24] and Bi_{0.9}Sb_{0.1} [25], as well as doping impurities into the heavy metal layer, including MgO [26], TiO₂ [27], Nb [28], and Hf [29], etc. On the other hand, H_c also exhibits a positive correlation with I_c based on the domain-wall depinning model [30–32], while this remains largely unexplored.

In this study, multilayer structures of Ta/(Pt¹/Ta)_n/Pt²/Co/Ta were grown by sputtering. It was found that the I_c of the sample with the superlattice buffer layer was significantly reduced through the anomalous Hall effect (AHE) and SOT switching measurements. The reduction in I_c mainly stems from two factors. Firstly, the increase in β_D is a result of the interfacial scattering introduced by the ultrathin metal interlayer [28,29]. Secondly, H_c has been reduced due to the decrease of the interfacial roughness by the superlattice buffer layer. Furthermore, it was discovered that I_c scales with H_c/β_D linearly. Most importantly, this linear relationship can be applied to many other metal dopants with the same superlattice structure.

*Contact author: ybxu@nju.edu.cn

†Contact author: heliang@nju.edu.cn

TABLE I. Thicknesses of each layer corresponding to different periods.

Sample name	A0	A1	A2	A3	A4	A5
Period (n)	N/A	1	2	3	4	5
Thickness of Pt ² (nm)	4	1.9	1.2	0.85	0.64	0.5
Thickness of Ta (nm)	0	0.2×1	0.2×2	0.2×3	0.2×4	0.2×5
Thickness of Pt ¹ (nm)	0	1.9×1	1.2×2	0.85×3	0.64×4	0.5×5

The multilayers of Ta/(Pt¹/Ta) _{n} /Pt²/Co/Ta were deposited on Si/SiO₂ substrates by magnetron sputtering with a base pressure of 3×10^{-7} Torr. The Ta layers at the bottom served as adhesion layers, while the superlattice buffer layers were responsible for generating spin current and imparting perpendicular magnetic anisotropy. The top Ta layer functioned as a protective cover, preventing the oxidation of the films. The diameters of all the targets are 50.8 mm. The purity of Ta target is 99.95%, while Pt and Co are 99.99%. The sputtering gas used is 99.999% Ar for all the materials. For material deposition, the pressure is kept at 6 mTorr and the dc power remains at 10 W. The deposition rates are 0.16 Å/s, 0.2 Å/s, and 0.14 Å/s for Ta, Pt, and Co layers, respectively. During deposition, the substrates were kept at room temperature.

The as-grown samples are shown in Table I with the specific names and thicknesses of each layer. The structure of the Sample A-series is illustrated in Fig. 1(a). The control samples of B-series, i.e., Ta₃/(Pt_x:Ta_{0.2}) _{n} /Pt_x/Co₁/Ta₂,

and C, i.e., Ta₃/Pt_{3.16}/Ta_{0.2}/Pt_{0.64}/Co₁/Ta₂, are also discussed in this article. Sample A0 is the basic structure with a single Pt buffer layer, and samples A1–A4 have the superlattice buffer layer of (Pt¹/Ta) _{n} /Pt². Notably, the total thickness of (Pt¹/Ta) _{n} /Pt² was maintained constant at 4 nm throughout our experiments. The magnetization-hysteresis (M–H) and AHE loops indicate that all the samples (A0–A4) exhibit good perpendicular magnetic anisotropy, as shown in Figs. 1(b) and 1(c). On the other hand, sample A5 ($n=5$) in Fig. S1 in the Supplementary Material [33] demonstrates in-plane magnetic anisotropy.

The quantity H_c for all the samples was extracted from M–H and AHE loops. Within the margin of error, they are nearly identical, decreasing from 150 Oe to 57 Oe as the period increased from 0 to 4, as shown in Fig. 1(d). The quantity H_c is reduced by 62%; this can be attributed to the improved interfacial roughness of the buffer layer, as shown in Fig. S2 in the Supplementary Material [33]. It is found that the roughness decreases from 1.69 nm to 0.57 nm as n increases. The roughness is directly proportional to the number of pinning sites meaning that, as the roughness increases, so does the abundance of pinning sites, which subsequently hinders domain-wall motion, ultimately resulting in enhanced coercivity [34].

After deposition, the samples were fabricated into a cross-bar device [Fig. 2(a) inset] using standard photolithography and ion beam etching processes. The width of the current channel is 20 μm. Figure 2(a) presents the SOT switching loops of samples A0 and A4 under the applied magnetic fields of ±1000 Oe. Compared with ΔR of AHE [Fig. 1(c)], the two samples show

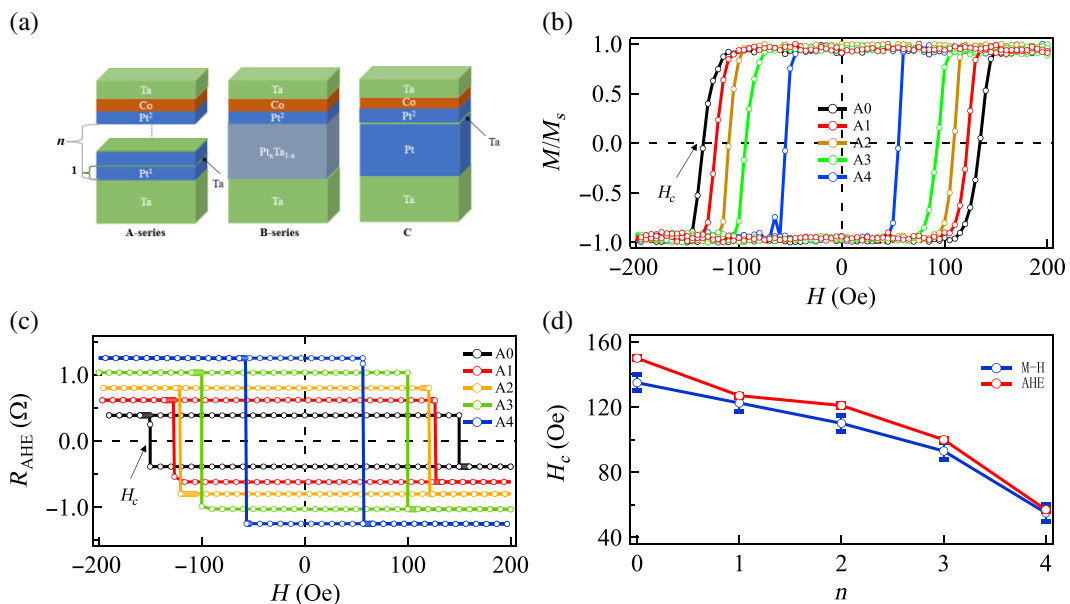


FIG. 1. (a) Structure of sample A-series, B-series, and C. (b) Normalized M–H loops and (c) AHE loops of Samples A0–A4 demonstrate out-of-plane easy axes. (d) The quantity H_c is extracted from M–H and AHE loops as a function of the period.

a complete switching ratio close to 100%. The quantity I_c of A4 is significantly reduced by 79% compared with that of A0, achieving a value of $5.88 \times 10^6 \text{ A/cm}^2$. The quantity I_c value is relatively lower compared with $1.15 \times 10^7 \text{ A/cm}^2$ for $\text{Pt}_{0.7}(\text{MgO})_{0.3}$ at 1500 Oe [26], $1.4 \times 10^7 \text{ A/cm}^2$ for $(\text{Pt}/\text{Nb})_7$ at 1000 Oe [28], and $1.7 \times 10^7 \text{ A/cm}^2$ for $[\text{Pt}/\text{Hf}]_5$ at 3000 Oe [29]. Fig. 2(b) demonstrates the switching loops of sample A4 under different in-plane fields H_x , parallel to the current. The SOT switching loops act in a counterclockwise direction under a positive magnetic field and a clockwise direction under a negative magnetic field. Figure 2(c) exhibits the switching phase diagram of A4. The quantity I_c of A4 decreases with an increase in the external magnetic field, which is consistent with previously reported results [35,36].

To investigate the dampinglike torque (DLT) of the spin current induced by SOT, a second harmonic method was adopted, as shown in Fig. S3 in the Supplementary Material [33]. The magnetic field is applied along the x -direction, with a small inclination angle (φ_H) with respect to the film surface used to prevent the formation of multiple domains. An ac with a frequency of 133 Hz is applied along the x -direction. Simultaneously, the first (V_ω) and secondary ($V_{2\omega}$) harmonic signals are acquired through a dual-channel lock-in amplifier of OE1022D. Figures 3(a) and 3(b) show V_ω and $V_{2\omega}$ as a function of magnetic field H_x (with an ac of 1 mA) for samples A0 and A4, respectively. The longitudinal effective field (H_L) induced by SOT can be quantitatively extracted using the following

formula [37,38]:

$$H_L = \frac{\partial V_{2\omega}}{\partial H_x} / \frac{\partial^2 V_\omega}{\partial H_x^2} \quad (1)$$

The dampinglike effective field (H_D) generated by the current can be acquired by the following formula [39]:

$$H_D = -2 \frac{H_L + 2\xi H_L}{1 - 4\xi^2}, \quad (2)$$

where ξ is the ratio of planar Hall resistance to anomalous Hall resistance. In the Pt/Co system, planar Hall values are very small and are often neglected [23]. Thus, H_D can be simplified as $-2H_L$. The extracted H_D vs I_{ac} plots are shown in Fig. 3(c) for all the samples. All of them exhibit a linear dependence on the applied current. Moreover, the slopes (β_D) increase from $6.9 \times 10^{-6} \text{ Oe/(A/cm}^2)$ to $8.9 \times 10^{-6} \text{ Oe/(A/cm}^2)$, as the period increases from 0 to 4, as shown in Fig. 3(d).

To justify the dramatic decrease of I_c due to the superlattice buffer layer, control samples of B-series and C have been prepared. First, the B-series of samples, specifically $\text{Ta}_3/(\text{Pt}_x\text{:Ta}_{0.2})_n/\text{Pt}_x/\text{Co}_1/\text{Ta}_2$, has been grown through cosputtering of Pt and Ta, utilizing atomic ratios of 0.84:0.16 and 0.79:0.21 for the superlattice buffer layers, respectively, corresponding to samples A3 and A4. This structure is represented in Fig. 1(a). As shown in Figs. S5(a)–S5(d) in the Supplementary Material [33], the switching current of the samples at 1000 Oe were

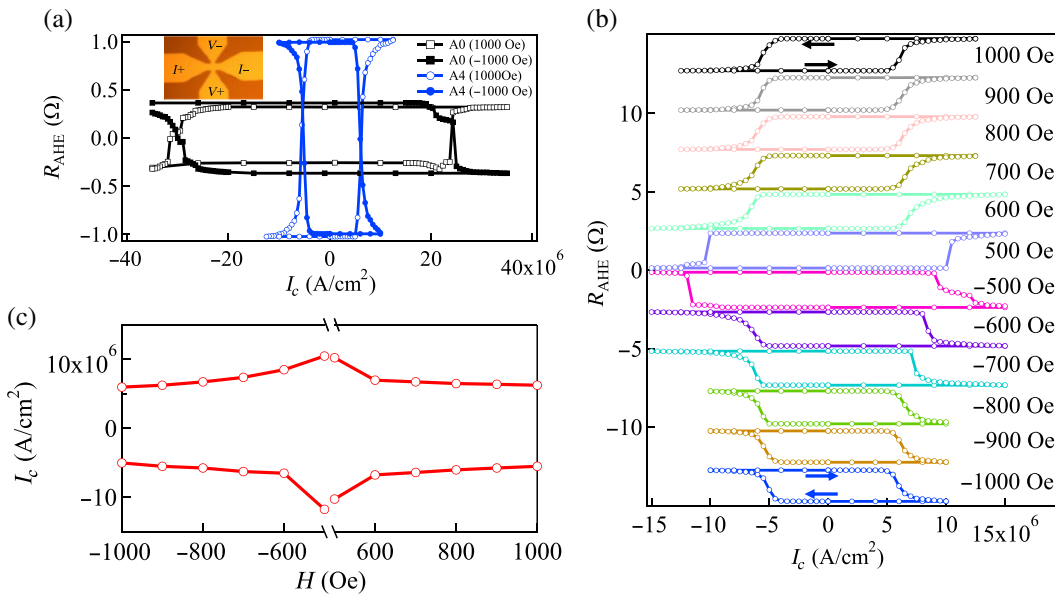


FIG. 2. Magnetic and SOT properties for the A0 and A4. (a) Current-induced magnetization switching in the A0 and A4 under an in-plane magnetic field of $H_x = \pm 1000 \text{ Oe}$. (b) Current-induced magnetization switching in A4 is observed under various in-plane magnetic fields H_x ranging from -1000 Oe to 1000 Oe . (c) Switching phase diagram of A4. The quantity I_c decreases as the applied magnetic field increases.

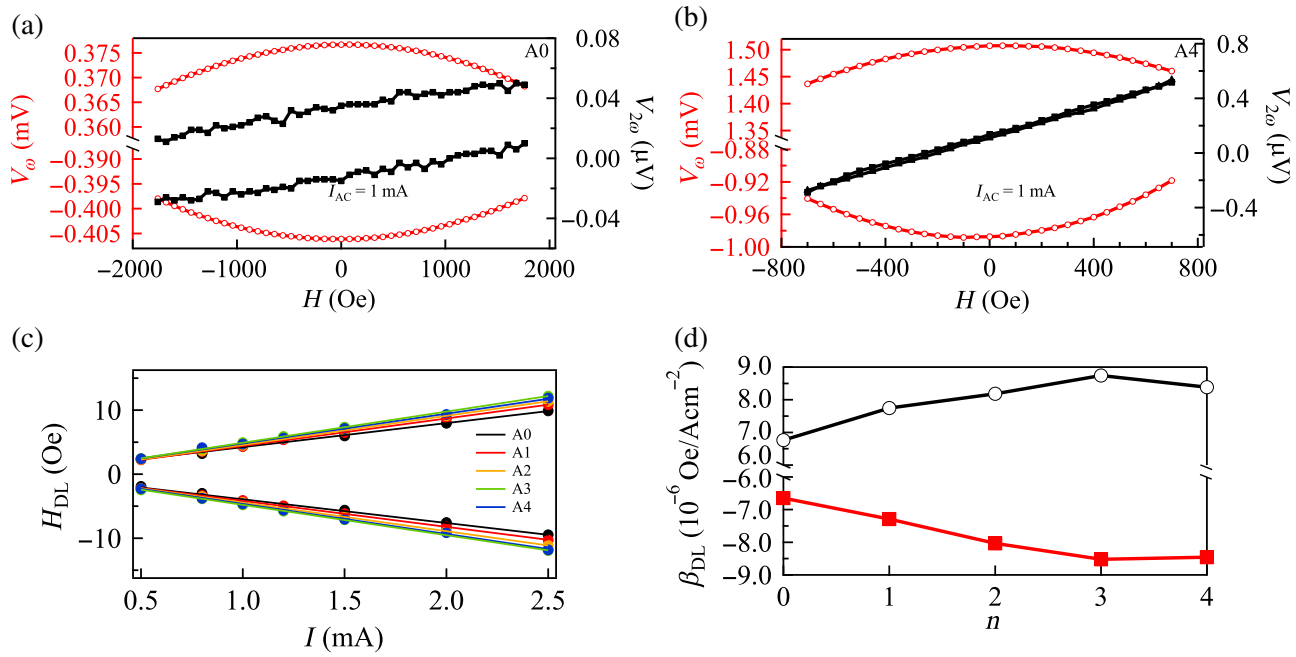


FIG. 3. Harmonic Hall measurements of the Hall-bar devices. The V_ω and $V_{2\omega}$ harmonic Hall voltages as a function of magnetic field H_x for (a) A0 and (b) A4. (c) Current dependence of H_D of A0–A4. (d) Variation of the dampinglike efficiency with different n .

2.05×10^7 and 1.33×10^7 A/cm 2 , much higher than that of A3 and A4, respectively. Second, Fig. 1(a) shows a sample C of Ta₃/Pt_{3.16}/Ta_{0.2}/Pt_{0.64}/Co₁/Ta₂ that has been deposited to demonstrate the effect of a Ta interlayer. The insertion of 0.2-nm Ta near Co resulted in a decrease in I_c of 20.4% for sample A0, which was still significantly lower than the previous value of 79%, as shown in Figs. S5(e) and S5(f) in the Supplementary Material [33]. Thus, the superlattice buffer layer is the main reason for reducing I_c .

In order to further clarify the underlying mechanism of the significant reduction of I_c , we here analyze the effects of H_c and β_D on I_c . Based on the domain-wall depinning

model, we find [31,40–42]

$$I_c = \frac{2e}{\hbar} \mu_0 M_s (t_{FM} - t_{dead}) \left(\frac{2}{\pi} \right) \left(\frac{H_c}{\beta_D} \right).$$

In our samples, e , \hbar , μ_0 , M_s , t_{FM} , and π are all constants; thus, we have $I_c \propto H_c/\beta_D$. Here, the coercivity (H_c) constitutes a pivotal component of the switching barrier, which is directly proportional to the difficulty of domain nucleation; hence, an increase in H_c corresponds to a heightened challenge to initiate domain nucleation. Furthermore, the parameter β_D exhibits a positive correlation with domain-wall propagation, suggesting that a higher β_D

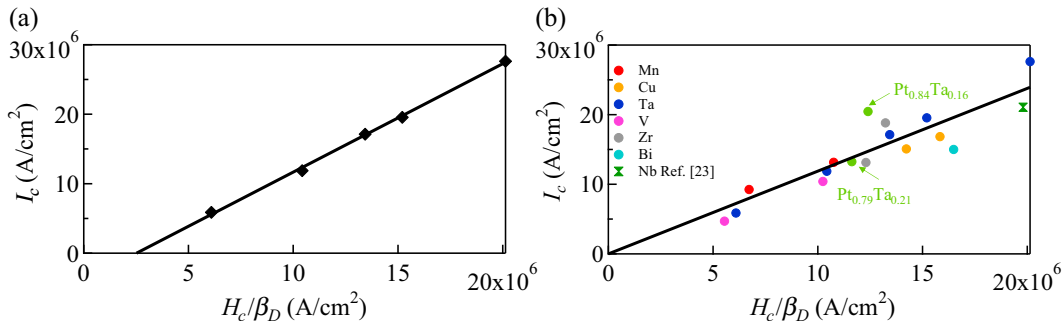


FIG. 4. (a) Relationship between I_c and H_c/β_D for sample A-series. (b) The I_c versus H_c/β_D relationship for various metal inserts, including Ta, Zr, Mn, V, Cu, Bi, and cosputtered Pt_xTa_{1-x}, exhibiting linear trends.

value translates to a more rapid propagation rate. Consequently, the ratio H_c/β_D effectively represents the balance between domain nucleation and domain-wall propagation.

A plot of I_c vs H_c/β_D is shown in Fig. 4(a). A perfect linear correlation is seen in Fig. 4(a), with all the points located on a straight line. To further corroborate this relationship, more samples with a $(\text{Pt}/X)_n$ superlattice buffer layer ($X = \text{Mn}, \text{Cu}, \text{V}, \text{Zr}$, and Bi , $n = 3$ or 4) have been prepared. The quantities I_c , β_D , and H_c were extracted from the AHE and SOT measurements, as shown in Fig. S4 in the Supplementary Material [33]. Figure 4(b) exhibits the same linear relationship between I_c and H_c/β_D for all the samples, including data from ref. [23]. This provides strong evidence of the validation of the domain-wall depinning model with the linear relationship between I_c and H_c/β_D .

In summary, by utilizing the superlattice buffer layer, I_c has been reduced by 79% compared with a pure Pt buffer layer. The reduction in I_c can be attributed to the increase in β_D due to the interface scattering and the reduction in H_c because of the decrease in the roughness of the Pt/Co interface. Moreover, I_c has been found to scale with H_c/β_D linearly, conforming to the domain-wall depinning mechanism. Most importantly, samples with the same superlattice buffer layer structure using different metal layers follow the same trend. Our findings point out an effective way to reduce the critical switching current by increasing β_D and/or decreasing H_c . This approach exhibits considerable potential in practical applications for SOT-based spintronic devices.

The data that support the findings of this study are available from the corresponding author upon reasonable request.

ACKNOWLEDGMENTS

This work is supported by the National Natural Science Foundation of China (Grant No. 12241403), the National Natural Science Foundation of China (Grants No. T2394473 and No. T2394470), and the Natural Science Foundation of Jiangsu Province of China (Grant No. BK20140054).

The authors declare no conflict of interest.

-
- [1] B. Cui, A. Chen, X. Zhang, B. Fang, Z. Zeng, P. Zhang, J. Zhang, W. He, G. Yu, P. Yan, X. Han, K. L. Wang, X. Zhang, and H. Wu, Low-power and field-free perpendicular magnetic memory driven by topological insulators, *Adv. Mater.* **35** (31), 2302350 (2023).
 - [2] X. Qiu, Z. Shi, W. Fan, S. Zhou, and H. Yang, Characterization and manipulation of spin orbit torque in magnetic heterostructures, *Adv. Mater.* **30** (17), 1705699 (2018).
 - [3] F. Xue, S.-J. Lin, M. Song, W. Hwang, C. Klewe, C.-M. Lee, E. Turgut, P. Shafer, A. Vailionis, Y.-L. Huang, W.

Tsai, X. Bao, and S. X. Wang, Field-free spin-orbit torque switching assisted by in-plane unconventional spin torque in ultrathin $[\text{Pt}/\text{Co}]_N$, *Nat. Commun.* **14** (1), 3932 (2023).

- [4] Y. Zhang, *et al.*, Room temperature field-free switching of perpendicular magnetization through spin-orbit torque originating from low-symmetry type II Weyl semimetal, *Sci. Adv.* **9** (44), 9819 (2023).
- [5] X. Zhan, H. Wang, Z. Li, and R. Liu, Significant enhancement of spin-orbit torque efficiency by optimizing the interlayer thickness in $[\text{Pt}/\text{Ru}]_n/\text{Pt}$ multilayers, *Appl. Phys. Lett.* **124** (7), 072406 (2024).
- [6] C. Grezes, A. Kandazoglou, M. Cosset-Cheneau, L. M. V. Arche, P. Noël, P. Sgarro, S. Auffret, K. Garello, M. Bibes, L. Vila, and J.-P. Attané, Non-volatile electric control of spin-orbit torques in an oxide two-dimensional electron gas, *Nat. Commun.* **14** (1), 2590 (2023).
- [7] H. Wu, A. Chen, P. Zhang, H. He, J. Nance, C. Guo, J. Sasaki, T. Shirokura, P. N. Hai, B. Fang, S. A. Razavi, K. Wong, Y. Wen, Y. Ma, G. Yu, G. P. Carman, X. Han, X. Zhang, and K. L. Wang, Magnetic memory driven by topological insulators, *Nat. Commun.* **12** (1), 6251 (2021).
- [8] L. Ren, L. Liu, X. Shu, W. Lin, P. Yang, J. Chen, and K. L. Teo, Spin-orbit torque switching of a high-quality perpendicularly magnetized ferrimagnetic Heusler Mn_3Ge film, *ACS Appl. Mater. Interfaces* **13** (15), 18294 (2021).
- [9] J. Ryu, S. Lee, K. Lee, and B. Park, Current-induced spin-orbit torques for spintronic applications, *Adv. Mater.* **32** (35), 1907148 (2020).
- [10] H. Ju, X. Zhao, W. Liu, Y. Song, L. Liu, J. Ma, Y. Li, J. Wu, and Z. Zhang, Enhanced spin-orbit torque and low critical current density in $\text{Pt}_{100-x}\text{Ru}_x/[\text{CoNi}]/\text{Ru}$ multilayer for spintronic devices, *ACS Appl. Mater. Interfaces* **13** (51), 61742 (2021).
- [11] A. Manchon, J. Zelezny, I. M. Miron, T. Jungwirth, J. Sinova, A. Thiaville, K. Garello, and P. Gambardella, Current-induced spin-orbit torques in ferromagnetic and antiferromagnetic systems, *Rev. Mod. Phys.* **91** (3), 035004 (2019).
- [12] T.-Y. Chen, W.-B. Liao, T.-Y. Chen, T.-Y. Tsai, C.-W. Peng, and C.-F. Pai, Current-induced spin-orbit torque efficiencies in W/Pt/Co/Pt heterostructures, *Appl. Phys. Lett.* **116** (7), 072405 (2020).
- [13] J. Yu, X. Qiu, W. Legrand, and H. Yang, Large spin-orbit torques in Pt/Co-Ni/W heterostructures, *Appl. Phys. Lett.* **109** (4), 042403 (2016).
- [14] C.-F. Pai, M.-H. Nguyen, C. Belvin, L. H. Vilela-Leão, D. C. Ralph, and R. A. Buhrman, Enhancement of perpendicular magnetic anisotropy and transmission of spin hall effect induced spin currents by a Hf spacer layer in W/Hf/CoFeB/MgO layer structures, *Appl. Phys. Lett.* **104** (8), 082407 (2014).
- [15] S. Fukami, C. Zhang, S. DuttaGupta, A. Kurenkov, and H. Ohno, Magnetization switching by spin-orbit torque in an antiferromagnet–ferromagnet bilayer system, *Nat. Mater.* **15** (5), 535 (2016).
- [16] Y.-W. Oh, S. Chris Baek, Y. M. Kim, H. Y. Lee, K.-D. Lee, C.-G. Yang, E.-S. Park, K.-S. Lee, K.-W. Kim, G. Go, J.-R. Jeong, B.-C. Min, H.-W. Lee, K.-J. Lee, and B.-G. Park, Field-free switching of perpendicular magnetization through spin-orbit torque in antiferromagnet/ferromagnet/oxide structures, *Nat. Nanotechnol.* **11** (10), 878 (2016).

- [17] L. Liu, C. Zhou, X. Shu, C. Li, T. Zhao, W. Lin, J. Deng, Q. Xie, S. Chen, J. Zhou, R. Guo, H. Wang, J. Yu, S. Shi, P. Yang, S. Pennycook, A. Manchon, and J. Chen, Symmetry-dependent field-free switching of perpendicular magnetization, *Nat Nanotechnol.* **16** (3), 277 (2021).
- [18] L. Liu, *et al.*, Current-induced self-switching of perpendicular magnetization in CoPt single layer, *Nat. Commun.* **13** (1), 3539 (2022).
- [19] H. Kim, K. Moon, B. X. Tran, S. Yoon, C. Kim, S. Yang, J. Ha, K. An, T. Ju, J. Hong, and C. Hwang, Field-free switching of magnetization by tilting the perpendicular magnetic anisotropy of Gd/Co multilayers, *Adv. Funct. Mater.* **32** (26), 2112561 (2022).
- [20] L. You, O. Lee, D. Bhowmik, D. Labanowski, J. Hong, J. Bokor, and S. Salahuddin, Switching of perpendicularly polarized nanomagnets with spin orbit torque without an external magnetic field by engineering a tilted anisotropy, *Proc. Natl. Acad. Sci. U.S.A.* **112** (33), 10310 (2015).
- [21] T.-Y. Chen, H.-I. Chan, W.-B. Liao, and C.-F. Pai, Current-induced spin-orbit torque and field-free switching in Mo-based magnetic heterostructures, *Phys. Rev. Appl.* **10** (4), 044038 (2018).
- [22] A. Razavi, H. Wu, B. Dai, H. He, D. Wu, K. Wong, G. Yu, and K. L. Wang, Spin-orbit torques in structures with asymmetric dusting layers, *Appl. Phys. Lett.* **117** (18), 182403 (2020).
- [23] S. Wang, X. Dai, K. He, J. Wang, X. Zhang, Q. Guo, G. Feng, Y. Xu, Y. Deng, R. Liu, J. Du, Y.-L. Wang, C. Wang, Y. Xu, and L. He, Field-free switching in perpendicular Ta/CoFeB/MgO multilayers achieved by annealing temperature gradient, *Appl. Phys. Lett.* **124** (11), 112415 (2024).
- [24] A. R. Mellnik, J. S. Lee, A. Richardella, J. L. Grab, P. J. Mintun, M. H. Fischer, A. Vaezi, A. Manchon, E.-A. Kim, N. Samarth, and D. C. Ralph, Spin-transfer torque generated by a topological insulator, *Nature* **511** (7510), 449 (2014).
- [25] N. H. D. Khang, Y. Ueda, and P. N. Hai, A conductive topological insulator with large spin Hall effect for ultralow power spin-orbit torque switching, *Nat. Mater.* **17** (9), 808 (2018).
- [26] L. Zhu, L. Zhu, M. Sui, D. C. Ralph, and R. A. Buhrman, Variation of the giant intrinsic spin Hall conductivity of Pt with carrier lifetime, *Sci. Adv.* **5** (7), 8025 (2019).
- [27] X. Xu, D. Zhang, B. Liu, H. Meng, J. Xu, Z. Zhong, X. Tang, H. Zhang, and L. Jin, Giant extrinsic spin Hall effect in platinum-titanium oxide nanocomposite films, *Adv. Sci.* **9** (16), 2105726 (2022).
- [28] J. Y. Zhang, P. W. Dou, R. Y. Liu, Y. B. Wang, X. Deng, L. Y. Feng, X. Q. Zheng, H. Huang, and S. G. Wang, Enhanced spin orbit torque efficiency induced by large skew scattering in perpendicular Pt/Co/Ta multilayers with superlattice/alloying Nb(Ir) insertion, *Appl. Phys. Lett.* **123** (18), 182401 (2023).
- [29] L. Zhu, L. Zhu, S. Shi, M. Sui, D. C. Ralph, and R. A. Buhrman, Enhancing spin-orbit torque by strong interfacial scattering from ultrathin insertion layers, *Phys. Rev. Appl.* **11** (6), 061004 (2019).
- [30] A. Thiaville, S. Rohart, É. Jué, V. Cros, and A. Fert, Dynamics of Dzyaloshinskii domain walls in ultrathin magnetic films, *Europhys. Lett.* **100**, 57002 (2012).
- [31] D. Bhowmik, M. E. Nowakowski, L. You, O. Lee, D. Keating, M. Wong, J. Bokor, and S. Salahuddin, Deterministic domain wall motion orthogonal to current flow due to spin orbit torque, *Sci. Rep.* **5**, 11823 (2015).
- [32] T.-Y. Chen, C.-T. Wu, H.-W. Yen, and C.-F. Pai, Tunable spin-orbit torque in Cu-Ta binary alloy heterostructures, *Phys. Rev. B* **96**, 104434 (2017).
- [33] See Supplementary Material <http://link.aps.org/supplemental/10.1103/PhysRevApplied.22.L021002> for the interface roughness of sample A-series, the schematic diagram of harmonic Hall measurements, harmonic data of different samples with various currents, the anomalous Hall effect, and the SOT switching of samples A, B, and C.
- [34] V. D. Duong, P. Cao Van, T. Nguyen Thi, H. Y. Ahn, V. A. Cao, J. Nah, G. Kim, K.-S. Lee, J.-W. Kim, and J.-R. Jeong, Interfacial roughness driven manipulation of magnetic anisotropy and coercivity in ultrathin thulium iron garnet films, *J. Alloys Compd.* **927**, 166800 (2022).
- [35] L. Liu, Y. Song, X. Zhao, W. Liu, and Z. Zhang, Full-scale field-free spin-orbit torque switching in HoCo structure with a vertical composition gradient, *Adv. Funct. Mater.* **32** (39), 2200328 (2022).
- [36] H. Wang, H. Wu, J. Zhang, Y. Liu, D. Chen, C. Pandey, J. Yin, D. Wei, N. Lei, S. Shi, H. Lu, P. Li, A. Fert, K. L. Wang, T. Nie, and W. Zhao, Room temperature energy-efficient spin-orbit torque switching in two-dimensional van der Waals Fe₃GeTe₂ induced by topological insulators, *Nat. Commun.* **14** (1), 5173 (2023).
- [37] J. Kim, J. Sinha, M. Hayashi, M. Yamanouchi, S. Fukami, T. Suzuki, S. Mitani, and H. Ohno, Layer thickness dependence of the current-induced effective field vector in Ta/CoFeB/MgO, *Nat. Mater.* **12** (3), 240 (2013).
- [38] Y. Li, X. Zhao, W. Liu, J. Wu, L. Liu, Y. Song, J. Ma, and Z. Zhang, Voltage-gated field-free spin-orbit torque switching in Pt/Co/Ir/MgO wedged structures, *Appl. Phys. Lett.* **123** (3), 032403 (2023).
- [39] T.-Y. Tsai, T.-Y. Chen, C.-T. Wu, H.-I. Chan, and C.-F. Pai, Spin-orbit torque magnetometry by wide-field magneto-optical Kerr effect, *Sci. Rep.* **8** (1), 5613 (2018).
- [40] A. Thiaville, S. Rohart, É. Jué, V. Cros, and A. Fert, Dynamics of Dzyaloshinskii domain walls in ultrathin magnetic films, *Europhys. Lett.* **100** (5), 2611 (2012).
- [41] T. Y. Chen, C. T. Wu, H. W. Yen, and C. F. Pai, Tunable spin-orbit torques in cu-ta binary alloy heterostructures, *Phys. Rev. B* **96** (10), 104434 (2017).
- [42] L. Zhu, Switching of perpendicular magnetization by spin-orbit torque, *Adv. Mater.* **35**, 2300853 (2023).